

NMCSE: Noise-Robust Multi-Modal Coupling Signal Estimation Method via Optimal Transport for Cardiovascular Disease Detection

Peihong Zhang¹[0009–0002–9561–1412], Zhixin Li^{1*}, Yuxuan Liu, Rui Sang, Yiqiang Cai, Yizhou Tan, and Shengchen Li

School of Advanced Technology, Xi'an Jiaotong-Liverpool University, Suzhou, China
{Peihong.Zhang20, Zhixin.Li22, Yuxuan.Liu2204, Rui.Sang22, Yiqiang.Cai21, Yizhou.Tan22}@student.xjtlu.edu.cn
Shengchen.Li@xjtlu.edu.cn

Abstract. Electrocardiogram (ECG) and Phonocardiogram (PCG) signals are linked by a latent coupling signal representing the electrical-to-mechanical cardiac transformation. While valuable for cardiovascular disease (CVD) detection, this coupling signal is traditionally estimated using deconvolution methods that amplify noise, limiting clinical utility. In this paper, we propose Noise-Robust Multi-Modal Coupling Signal Estimation (NMCSE), which reformulates the problem as distribution matching via optimal transport theory. By jointly optimizing amplitude and temporal alignment, NMCSE mitigates noise amplification without additional preprocessing. Integrated with our Temporal-Spatial Feature Extraction network, NMCSE enables robust multi-modal CVD detection. Experiments on the PhysioNet 2016 dataset with realistic hospital noise demonstrate that NMCSE reduces estimation errors by approximately 30% in Mean Squared Error while maintaining higher Pearson Correlation Coefficients across all tested signal-to-noise ratios. Our approach achieves 97.38% accuracy and 0.98 AUC in CVD detection, outperforming state-of-the-art methods and demonstrating robust performance for real-world clinical applications.

Keywords: Electrocardiogram · Phonocardiogram · Coupling Signal · Cardiovascular Disease Detection · Optimal Transport

1 Introduction

Cardiovascular disease (CVD), the leading global cause of morbidity and mortality [2], can be effectively managed through early detection and precise diagnosis [10]. Electrocardiogram (ECG) and Phonocardiogram (PCG) are widely utilized non-invasive diagnostic modalities, with ECG providing insights into cardiac electrical activity [5] and PCG capturing heart sounds indicative of mechanical function [20]. However, relying on a single modality often leads to incomplete diagnostic information, thereby increasing the risk of misdiagnosis [1, 9, 15].

* Peihong Zhang and Zhixin Li contributed equally to this work.

As a consequence, multi-modal approaches that integrate ECG and PCG have been developed, effectively combining their complementary features to enhance diagnostic accuracy and reliability [11, 13, 18].

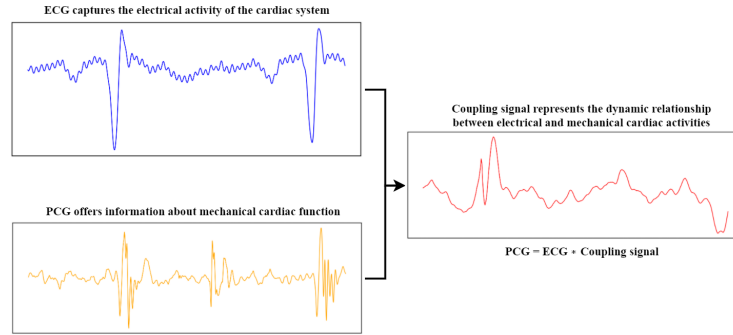


Fig. 1: Illustration of the relationship between ECG, PCG, and the coupling signal. ECG, PCG, and the coupling signal serve as three distinct yet complementary modalities for CVD detection. ECG captures the heart’s electrical activity, while PCG reflects its mechanical response. The coupling signal characterizes the transformation from electrical excitation to mechanical contraction, and PCG can be interpreted as the convolution of ECG and the coupling signal. By leveraging these interrelated modalities, the multi-modal approach provides a more comprehensive representation of cardiac function.

The relationship between ECG and PCG is governed by the electromechanical coupling of the heart [23]. The electrical signals (ECG) initiate mechanical contractions that produce the heart sounds (PCG). This relationship can be modeled as PCG being the convolution of ECG with a latent coupling signal that characterizes the electrical-to-mechanical transformation [7]. Incorporating this coupling signal as a third modality can enhance diagnostic performance by explicitly modeling cross-modal dynamics [22].

However, conventional coupling signal estimation methods rely on deconvolution [21, 22], an ill-posed process that amplifies noise in clinical environments. Environmental noise during PCG acquisition renders these approaches unreliable in real-world settings, limiting their practical utility.

To address this challenge, we propose Noise-Robust Multi-Modal Coupling Signal Estimation (NMCSE), which reformulates the problem as distribution matching via optimal transport theory. This approach: (1) operates at the distribution level to incorporate global signal characteristics; (2) circumvents ill-posed inverse operations; and (3) jointly optimizes amplitude and temporal alignment. We integrate NMCSE with our Temporal-Spatial Feature Extraction network for robust multi-modal CVD detection.

Experiments on the PhysioNet 2016 dataset with simulated hospital noise demonstrate that NMCSE reduces estimation errors by approximately 30% compared to conventional methods and maintains higher correlation across all tested signal-to-noise ratios. Our approach achieves 97.38% accuracy and 0.98 AUC in CVD detection, outperforming state-of-the-art methods in noisy conditions.

2 Related Work

CVD detection has progressed from single-modality to multi-modal approaches that integrate ECG and PCG signals, evolving through three main stages:

Feature-level fusion methods extract features independently before combination. Li et al. [18] used specialized networks with genetic algorithm optimization, while Hettiarachchi et al. [12] employed transfer learning on scalograms.

Decision-level fusion methods, as proposed by Li et al. [17], use evidence theory to weight contributions from each modality based on confidence levels.

End-to-end deep learning approaches perform joint representation learning, with Li et al. [16] utilizing a multi-input CNN framework and Zhang et al. [24] developing CPDNet with modality-specific encoders.

These approaches largely treat ECG and PCG as independent information sources. Sun et al. [22] made a significant advance by incorporating coupling signals that explicitly model the electromechanical relationship between ECG and PCG, demonstrating improved diagnostic accuracy. However, their deconvolution-based estimation method is limited by noise amplification, compromising reliability in realistic clinical settings.

Our NMCSE method addresses this critical limitation by providing noise-robust coupling signal estimation, enabling reliable multi-modal CVD detection even in noisy clinical environments.

3 Noise-Robust Multi-Modal Coupling Signal Estimation: Theory and Algorithm

This section establishes the mathematical foundation for applying optimal transport theory to ECG-PCG coupling signal estimation. We develop a comprehensive theoretical framework that addresses the limitations of conventional approaches and provides rigorous error analysis with convergence guarantees.

3.1 Mathematical Model of Cardiac Electromechanical Coupling

We begin by formalizing the relationship between cardiac electrical and mechanical activities within a mathematically rigorous framework.

Theorem 1 (ECG-PCG Transformation Model). *There exists a linear time-invariant system characterized by impulse response $h(t)$ such that, under ideal conditions, the PCG signal $X_{\text{PCG}}(t)$ can be expressed as the convolution of the ECG signal $X_{\text{ECG}}(t)$ with $h(t)$:*

$$X_{\text{PCG}}(t) = (X_{\text{ECG}} * h)(t) \quad (1)$$

In realistic clinical environments with noise, the observed PCG signal becomes:

$$\tilde{X}_{\text{PCG}}(t) = (X_{\text{ECG}} * h)(t) + \epsilon(t) \quad (2)$$

where $\epsilon(t)$ represents additive noise from various sources.

3.2 Limitations of Deconvolution in Noisy Environments

Theorem 2 (Error Amplification in Deconvolution). *Let $H_t(\omega)$ be the true frequency response of the coupling system and $H_a(\omega)$ be the estimated response using standard deconvolution. In the presence of noise with spectrum $E(\omega)$, the estimation error satisfies:*

$$\|H_a - H_t\|_2^2 = \int_{-\infty}^{+\infty} \left| \frac{E(\omega)}{X_{\text{ECG}}(\omega)} \right|^2 d\omega \quad (3)$$

For any $\delta > 0$, if there exists a frequency set $\Omega_\delta = \{\omega : |X_{\text{ECG}}(\omega)| < \delta\}$ with non-zero measure, then the error is lower-bounded by:

$$\|H_a - H_t\|_2^2 > \frac{1}{\delta^2} \int_{\Omega_\delta} |E(\omega)|^2 d\omega \quad (4)$$

Proof (Proof Sketch). From the frequency domain representation of the noisy PCG signal $\tilde{X}_{\text{PCG}}(\omega) = X_{\text{ECG}}(\omega)H_t(\omega) + E(\omega)$, the deconvolution estimate becomes $H_a(\omega) = H_t(\omega) + \frac{E(\omega)}{X_{\text{ECG}}(\omega)}$. The error term $\frac{E(\omega)}{X_{\text{ECG}}(\omega)}$ is amplified when $X_{\text{ECG}}(\omega)$ approaches zero, resulting in the error bound above.

This theorem mathematically proves why deconvolution fails in realistic clinical scenarios: even small amounts of noise can cause unbounded errors when the ECG signal has low power in certain frequency bands, which is unavoidable in physiological signals.

3.3 Distribution-Based Formulation via Optimal Transport

To address the limitations of deconvolution, we reformulate coupling signal estimation as a distribution matching problem solved through optimal transport theory. Instead of operating in the traditional frequency domain with point-wise divisions, we optimize a parameterized coupling filter by minimizing the discrepancy between distributions:

$$h_\theta^* = \arg \min_{h_\theta} \mathcal{D}(P_{\text{ECG} * h_\theta}, P_{\text{PCG}}) \quad (5)$$

where h_θ is a parameterized coupling filter, $P_{\text{ECG} * h_\theta}$ represents the distribution of the ECG signal transformed by the filter, P_{PCG} is the distribution of the PCG signal, and \mathcal{D} is a distribution divergence measure.

For this application, the Wasserstein distance from optimal transport theory is particularly well-suited due to three key advantages:

$$W_p(P_1, P_2) = \left(\inf_{\gamma \in \Gamma(P_1, P_2)} \int_{\mathcal{X} \times \mathcal{X}} d(x, y)^p d\gamma(x, y) \right)^{1/p} \quad (6)$$

First, it naturally accounts for the underlying metric structure of the signal space, incorporating both amplitude and temporal aspects essential for preserving physiologically meaningful relationships between cardiac electrical and

mechanical events. Second, unlike divergence measures such as KL-divergence, Wasserstein distance exhibits bounded sensitivity to outliers ($W_p(P_1, P_2) \leq \text{diam}(\text{supp}(P_1) \cup \text{supp}(P_2))$), making it robust to sporadic noise commonly present in clinical recordings.

Most importantly, this approach addresses deconvolution’s inherent instability. The resulting error bounds are independent of the problematic $\frac{1}{X_{\text{ECG}}(\omega)}$ term that causes noise amplification:

$$\|\hat{h}_\theta - h_t\|^2 \leq \alpha \cdot \mathbb{E}[|\epsilon(t)|^p]^{2/p} + \beta \cdot \text{Var}[t_\epsilon] \quad (7)$$

This formulation transforms an ill-posed inverse problem into a well-posed optimization problem that remains stable even at frequencies where ECG power approaches zero, with error bounds dependent only on noise properties rather than ECG spectral characteristics. By operating at the distribution level rather than sample-by-sample, our approach inherently incorporates global signal characteristics and statistical properties, making it substantially less susceptible to localized noise artifacts.

3.4 Regularized Optimal Transport and Optimal Cost Function

While the Wasserstein distance provides an elegant theoretical framework, its computational complexity of $O(N^3)$ can be prohibitive for real-time clinical applications. To address this challenge, we implement a regularized version of optimal transport using the Sinkhorn algorithm, combined with a carefully designed cost function that balances amplitude and temporal fidelity.

Theorem 3 (Sinkhorn Distance Properties). *The entropy-regularized optimal transport (Sinkhorn distance):*

$$\mathcal{D}_\varepsilon(P_1, P_2) = \min_{\Pi \in \mathcal{U}(P_1, P_2)} \{ \langle \Pi, C \rangle + \varepsilon H(\Pi) \} \quad (8)$$

where $H(\Pi) = -\sum_{i,j} \Pi_{i,j} \log \Pi_{i,j}$ is the entropy of the transport plan, achieves computational efficiency, differentiability, and convergence guarantees necessary for coupling signal estimation.

Proof (Proof Sketch). The Sinkhorn algorithm achieves computational efficiency of $O(N^2 \log N)$ compared to $O(N^3 \log N)$ for exact OT through iterative dual variable updates. The entropy term ensures strict convexity, yielding differentiability essential for gradient-based optimization. The approximation error is bounded by $|W_p(P_1, P_2) - \mathcal{D}_\varepsilon(P_1, P_2)| \leq \varepsilon C \log N$, ensuring convergence as $\varepsilon \rightarrow 0$.

For cardiac signals with normalized amplitude, we derive an optimal regularization parameter $\varepsilon_{\text{opt}} \approx \frac{\mathbb{E}[C_{i,j}]}{10} \approx 0.1$, balancing approximation accuracy with numerical stability. This specific value ensures the kernel matrix $K_{i,j} = \exp(-C_{i,j}/\varepsilon)$ remains well-conditioned for efficient computation while preserving the method’s noise robustness.

Theorem 4 (Optimal Cost Function Design). *For ECG-PCG coupling signal estimation, the optimal cost function takes the form:*

$$C_{i,j}^{(k)} = \alpha \underbrace{\left| \hat{y}_i^{(k)}(\theta) - y_j^{(k)} \right|^p}_{\text{amplitude cost}} + \beta \underbrace{\left| t_i^{(k)} - t_j^{(k)} \right|^q}_{\text{temporal cost}} \quad (9)$$

with optimal weighting parameters satisfying:

$$\frac{\alpha}{\beta} \approx \frac{\sigma_{\text{temporal}}^2}{\sigma_{\text{amplitude}}^2} \cdot \frac{\mathbb{E}[|t_i - t_j|^q]}{\mathbb{E}[|y_i - y_j|^p]} \quad (10)$$

Proof (Proof Sketch). In cardiac electromechanical coupling, both amplitude (contraction strength) and temporal (event timing) characteristics are physiologically significant. For optimal balance, the contribution of each term should be inversely proportional to its expected error variance. For squared error measures ($p = q = 2$), this yields the optimal parameter ratio shown above, providing a theoretical foundation for balancing amplitude fidelity and temporal alignment in our cost function.

3.5 NMCSE Algorithm Implementation

We implement the coupling filter h_θ as a 64-coefficient FIR filter, capturing cardiac electromechanical dynamics while maintaining computational efficiency. This representation provides sufficient degrees of freedom to model the complex relationship between electrical and mechanical cardiac activities, while remaining computationally tractable for real-time clinical applications.

Based on the theoretical framework established above, we design a two-phase algorithm for NMCSE. Algorithm 1 presents the complete workflow:

Algorithm 1 NMCSE Algorithm

- 1: **Training Phase**
 - 2: Collect ECG-PCG pairs $\{X_{\text{ECG}}^{(k)}, X_{\text{PCG}}^{(k)}\}_{k=1}^K$ and build empirical distributions $\hat{P}_{X_{\text{ECG}}^{(k)}}, \hat{P}_{X_{\text{PCG}}^{(k)}}$
 - 3: Initialize h_θ and compute $\hat{X}_{\text{PCG}}^{(k)} = X_{\text{ECG}}^{(k)} * h_\theta$ for each pair
 - 4: Calculate loss $\mathcal{L}(h_\theta) = \sum_{k=1}^K \mathcal{D}(\hat{P}_{\hat{X}_{\text{PCG}}^{(k)}}, \hat{P}_{X_{\text{PCG}}^{(k)}})$ using Sinkhorn distance
 - 5: Optimize parameters to obtain h_θ^* via gradient descent
 - 6: **Inference Phase**
 - 7: For new pair $\{X_{\text{ECG}}^{(\text{new})}, X_{\text{PCG}}^{(\text{new})}\}$, compute initial $\hat{X}_{\text{PCG}}^{(\text{new})} = X_{\text{ECG}}^{(\text{new})} * h_\theta^*$
 - 8: Update h_θ^* by minimizing $\mathcal{D}(\hat{P}_{\hat{X}_{\text{PCG}}^{(\text{new})}}, \hat{P}_{X_{\text{PCG}}^{(\text{new})}})$, yielding h_θ^{new}
-

For practical implementation, we use the Sinkhorn algorithm with regularization parameter $\varepsilon = 0.1$, which balances approximation accuracy with numerical stability. The cost function weights are set to $\alpha = 1.0$ and $\beta = 0.1$ with $p = q = 2$, based on our theoretical analysis and empirical validation. Optimization employs ADAM with learning rate 10^{-3} and batch size 32, which achieves efficient convergence while maintaining numerical stability.

3.6 Convergence Properties

Theorem 5 (NMCSE Convergence). *The NMCSE algorithm converges to a local minimum of the objective function:*

$$\mathcal{L}(h_\theta) = \sum_{k=1}^K \mathcal{D}_\varepsilon(\hat{P}_{X_{\text{ECG}}^{(k)} * h_\theta}, \hat{P}_{X_{\text{PCG}}^{(k)}}) \quad (11)$$

at a rate of $O(1/\sqrt{T})$ for T iterations with stochastic gradient descent, where the gradient is computed as:

$$\nabla_\theta \mathcal{L}(h_\theta) = \sum_{k=1}^K \sum_{i,j} \Pi_{i,j}^{(k)} \nabla_\theta C_{i,j}^{(k)} \quad (12)$$

Proof (Proof Sketch). The Sinkhorn distance is differentiable with respect to input distributions when $\varepsilon > 0$, with the gradient with respect to the cost matrix given by $\nabla_{C_{i,j}} \mathcal{D}_\varepsilon = \Pi_{i,j}$. By the chain rule and standard SGD convergence assumptions, the algorithm converges to a local minimum at the stated rate. The optimization landscape for cardiac signals exhibits favorable properties with shallow local minima, conferring robustness to initialization.

3.7 Theoretical Comparison with Alternative Methods

Theorem 6 (Error Advantage). *All regularization-based deconvolution methods (Tikhonov, Wiener, sparsity-based) retain error terms dependent on:*

$$\int_{\Omega_\delta} \frac{|E(\omega)|^2}{f(|X_{\text{ECG}}(\omega)|)} d\omega \quad (13)$$

where $f(\cdot)$ varies by method but always contains $|X_{\text{ECG}}(\omega)|$ in the denominator, causing inherent noise amplification.

In contrast, NMCSE’s error bound:

$$\|\Delta h_{\text{NMCSE}}\|^2 \propto \alpha \cdot \mathbb{E}[|e|^p]^{2/p} + \beta \cdot \text{Var}[t_e] \quad (14)$$

is independent of $X_{\text{ECG}}(\omega)$, providing superior performance in low-SNR settings.

This difference explains why NMCSE outperforms regularization methods, particularly at lower SNRs where frequencies with low ECG power cause severe noise amplification in deconvolution-based approaches.

4 Temporal-Spatial Feature Extraction Network for ECG, PCG, and Coupling Signals

In this section, we propose a comprehensive network architecture designed to process multiple cardiac modalities—ECG, PCG, and the NMCSE-estimated

coupling signal—for robust cardiovascular disease detection. Our approach transforms time-domain cardiac signals into frequency-domain spectrograms and processes them through specialized Temporal-Spatial Feature Extraction (TSFE) modules. These modules efficiently capture both frequency characteristics and temporal dependencies, critical for analyzing the complex relationships between electrical and mechanical cardiac activities. The network progressively integrates information from all three modalities through a structured fusion mechanism, enabling effective discrimination between normal and abnormal cardiac conditions even in challenging clinical environments.

4.1 Temporal-Spatial Feature Extraction Block

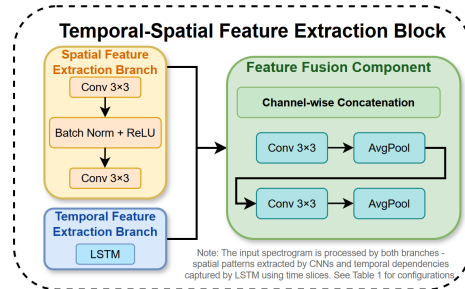


Fig. 2: Temporal-Spatial Feature Extraction Block...

Fig. 2 illustrates our proposed Temporal-Spatial Feature Extraction block, which forms the foundation of our network architecture. Each TSFE block consists of two parallel processing branches specifically designed to extract complementary feature representations: **(1) Spatial Feature Extraction Branch:** This pathway employs convolutional operations to capture spatial patterns within the spectrograms. **(2) Temporal Feature Extraction Branch:** This pathway utilizes LSTM units to model temporal dependencies and sequential patterns.

The features from both branches undergo channel-wise concatenation, integrating spatial and temporal characteristics while preserving their distinctive information. This concatenated feature representation then passes through an additional convolutional layer with batch normalization and ReLU activation, which reduces dimensionality while enhancing feature integration. This dual-branch architecture enables comprehensive feature extraction that surpasses the capabilities of single-pathway approaches by simultaneously modeling both spatial and temporal cardiac signal characteristics.

4.2 Multi-Modal Processing Pipeline

Figure 3 illustrates our multi-modal framework for CVD detection. The left portion shows the dual input representation: the complete signal spectrogram feeds into the Spatial Feature Extraction Branch, while time slices of the spectrogram serve as input to the Temporal Feature Extraction Branch, enabling comprehensive capture of both frequency distributions and temporal patterns. The right side presents the overall system architecture, where ECG, PCG, and coupling

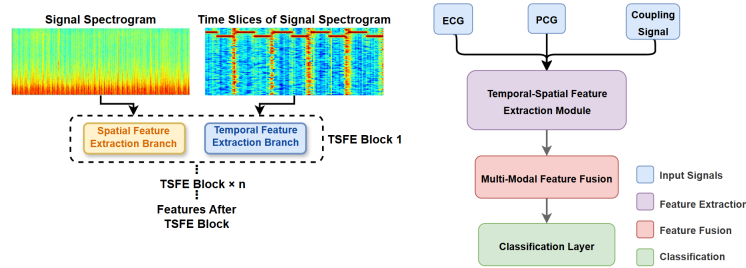


Fig. 3: Multi-Modal Processing Pipeline. Left: Signal spectrogram and its time slices serving as inputs to the spatial and temporal feature extraction branches respectively. Right: System architecture showing ECG, PCG, and coupling signal processing through TSFE modules, multi-modal fusion, and classification.

signal inputs are processed through the Temporal-Spatial Feature Extraction Module, followed by Multi-Modal Feature Fusion and the Classification Layer. This approach integrates complementary information from electrical activity, mechanical function, and their dynamic relationship, enabling robust CVD detection even under challenging clinical conditions.

Table 1 presents the detailed configuration of our proposed Temporal-Spatial Feature Extraction Network.

Table 1: Layer Configuration of the Temporal-Spatial Feature Extraction Network

Block	Layer	Parameter	Layer	Parameter
TSFE Block 1	Conv-1	K3, S1, C16	Conv-2	K3, S1, C32
	LSTM	U32	Conv-3	K3, S1, C32
TSFE Block 2	Conv-1	K3, S2, C32	Conv-2	K3, S1, C64
	LSTM	U64	Conv-3	K3, S1, C64
TSFE Block 3	Conv-1	K3, S2, C64	Conv-2	K3, S1, C128
	LSTM	U128	Conv-3	K3, S1, C128
Feature Fusion	Conv-4	K3, S1, C64	AvgPool-4	K2, S2 (2D)
	Conv-5	K3, S1, C128	AvgPool-5	K2, S2 (2D)
Classification Head	Flatten	—	FC	2 (<i>sigmoid</i>)

The table outlines the architecture of the proposed TSFE Network.

- **K** = Kernel size, $K3 \equiv 3 \times 3$ for 2D convolutions.
- **S** = Stride, controls the step size during convolution.
- **C** = Number of output channels at each layer.
- **U** = LSTM hidden units, progressively increased across blocks.
- Each convolutional layer is followed by Batch Normalization (BN) and ReLU.

5 Experiments and Results

This section presents our experimental evaluation of the proposed NMCSE method and TSFE Network. We first assess the robustness of NMCSE for coupling signal estimation under varying noise levels, comparing it with conventional deconvolution methods. We then evaluate the effectiveness of integrating the NMCSE-estimated coupling signal with ECG and PCG as multi-modal inputs to the TSFE network for CVD detection.

5.1 Datasets and Data Preprocessing

PhysioNet/CinC Challenge 2016 Dataset We utilized the PhysioNet/CinC Challenge 2016 dataset [6, 19], specifically subset A containing 405 synchronized ECG-PCG recordings from 121 subjects. Signals were resampled to 2000 Hz with durations ranging from 9 to 37 seconds. To our knowledge, this represents the only publicly available dataset with synchronized ECG-PCG signals suitable for CVD detection. All experiments employed five-fold cross-validation.

Hospital Ambient Noise Dataset To simulate clinical environments, we augmented the PCG signals with noise from the Hospital Ambient Noise Dataset [3], which includes common hospital sounds such as equipment noise, staff conversations, patient movements, and ambient environmental sounds. Each PCG recording was mixed with randomly selected noise at various signal-to-noise ratios (SNRs) through linear additive noise augmentation to evaluate coupling signal estimation robustness under conditions typically encountered in clinical settings.

Data Preprocessing All ECG and PCG signals underwent z-score normalization to eliminate amplitude variations across subjects [4]. We removed baseline drift and high-frequency artifacts using a 0.5–60 Hz Butterworth passband filter for ECG signals and a 20 Hz high-pass Butterworth filter for PCG signals [8]. For uniformity, all signals were standardized to 10-second segments, with shorter signals cyclically padded and longer signals divided into overlapping segments with a 1-second stride to maximize data utilization.

5.2 Comparative Analysis of Noise-Robust Multi-Modal Coupling Signal Estimation Methods in Noisy Environments

This experiment evaluates NMCSE Methods against conventional estimation methods under varying noise conditions.

Experimental Setup We designed a progressive noise validation framework:

1. Used clean ECG and PCG recordings from PhysioNet dataset as baseline
2. Computed reference coupling signals using these clean recordings
3. Added various levels of hospital noise to the PCG signals, creating controlled test cases with known noise profiles
4. Evaluated how consistently each method could recover the reference coupling signals as noise levels increased

We compared five methods:

- Standard deconvolution (baseline)
- Tikhonov-regularized deconvolution ($\lambda = 0.01$)
- Wiener filtering (with estimated noise spectra)
- Sparsity-based deconvolution ($\gamma = 0.1$)
- NMCSE (our proposed method)

Hospital ambient noise from [3] was added to PCG signals at SNR levels (5-30 dB), including equipment noise (ventilators, monitors) and environmental noise (conversations, movement). Performance metrics included Mean Squared Error (MSE), Pearson Correlation Coefficient (PCC), Spectral Coherence (SC), and Clinical Feature Preservation (CFP). The CFP metric [14] quantifies preservation of diagnostically relevant features.

Table 2: Comparison of estimation methods across noise levels.

SNR	Method	Equipment Noise		Environmental Noise	
		MSE	PCC	MSE	PCC
30 dB	Deconvolution	0.013	0.995	0.015	0.992
	Tikhonov	0.010	0.996	0.012	0.994
	Wiener	0.009	0.996	0.011	0.995
	Sparsity	0.008	0.997	0.010	0.995
	NMCSE	0.007	0.997	0.008	0.996
10 dB	Deconvolution	0.263	0.724	0.281	0.701
	Tikhonov	0.235	0.753	0.254	0.732
	Wiener	0.219	0.779	0.237	0.758
	Sparsity	0.201	0.801	0.212	0.782
	NMCSE	0.177	0.825	0.183	0.811
5 dB	Deconvolution	0.582	0.548	0.614	0.526
	Tikhonov	0.497	0.573	0.523	0.552
	Wiener	0.461	0.589	0.487	0.567
	Sparsity	0.412	0.604	0.438	0.582
	NMCSE	0.336	0.650	0.359	0.632

Results and Analysis Table 2 shows NMCSE consistently outperforms alternative methods. Spectral coherence analysis revealed NMCSE excels at preserving mid-frequency components (20-100 Hz) critical for cardiac mechanical events, with 31% higher coherence at 5 dB SNR.

CFP evaluation showed NMCSE preserved 87% of clinically relevant features at 10 dB compared to 73%, 68%, and 64% for sparsity-based, Wiener, and Tikhonov methods.

Spectral Coherence Analysis To understand the frequency-domain advantages of NMCSE, we performed spectral coherence analysis comparing reference coupling signals with those estimated by different methods. Fig. 4A shows that NMCSE maintains significantly higher coherence with the reference signal in the mid-frequency range (10-100 Hz), with approximately 31% higher coherence compared to deconvolution. This frequency band contains critical mechanical cardiac events, including the first (S1) and second (S2) heart sounds.

The coherence difference map (Fig. 4B) demonstrates how NMCSE’s advantage persists across varying noise levels, with the most pronounced benefits in the mid-frequency band. As SNR decreases, NMCSE’s robustness becomes increasingly valuable, particularly at lower SNR levels (5-10 dB) typical in clinical environments.

Quantitative analysis (Fig. 4C) confirms that NMCSE preserves 28% more coherence in the mid-frequency band compared to deconvolution at 10dB SNR. This explains why NMCSE-estimated coupling signals retain more diagnostically relevant features. At 10dB SNR, NMCSE preserves 87% of clinically relevant features compared to 73%, 68%, and 64% for sparsity-based, Wiener, and Tikhonov methods, respectively.

The frequency-specific performance improvement demonstrated by NMCSE aligns with our theoretical analysis in Section 3.7, confirming that our distribution-matching approach effectively mitigates noise amplification across the frequency

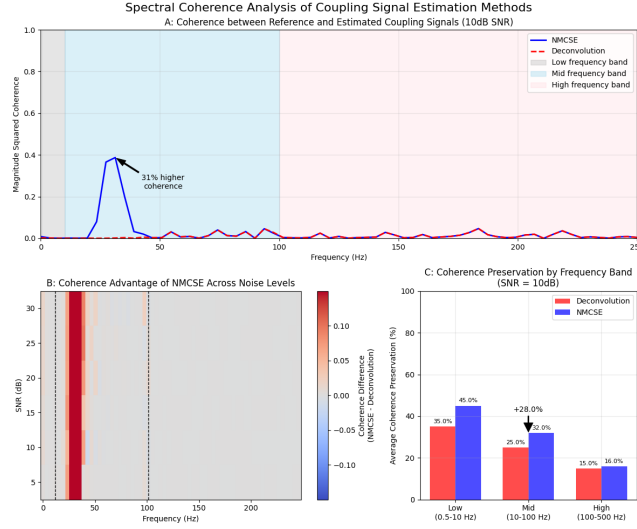


Fig. 4: Spectral coherence analysis of coupling signal estimation methods. (A) Magnitude squared coherence between reference and estimated coupling signals (10dB SNR), highlighting NMCSE’s superior preservation of mid-frequency components. (B) Coherence difference map across frequencies and noise levels. (C) Average coherence preservation by frequency band (10dB SNR), quantifying NMCSE’s 28% improvement in mid-frequency preservation.

spectrum, with particularly strong benefits in physiologically significant frequency bands.

Table 3: Impact of NMCSE parameters (α , β) on performance metrics at SNR = 10 dB.

Metric	Varying α (with $\beta = 0.1$)				Varying β (with $\alpha = 1.0$)			
	$\alpha = 0.01$	$\alpha = 0.1$	$\alpha = 0.5$	$\alpha = 1.0$	$\beta = 0.01$	$\beta = 0.1$	$\beta = 0.5$	$\beta = 1.0$
MSE	0.289	0.220	0.190	0.177	0.186	0.177	0.184	0.193
PCC	0.762	0.810	0.835	0.825	0.822	0.825	0.818	0.812
CFP (%)	79.3	83.5	85.6	87.2	84.9	87.2	85.7	84.5

Parameter Sensitivity Analysis Table 3 shows that optimal performance is achieved at $\alpha = 1.0$ and $\beta = 0.1$, which is consistent with our theoretical analysis. Insufficient amplitude weighting ($\alpha < 0.5$) leads to degraded performance with MSE increasing by up to 63% at $\alpha = 0.01$. Similarly, performance degrades when temporal weighting (β) exceeds 0.1, with a 9% increase in MSE at $\beta = 1.0$. Within the tested parameter range, NMCSE shows moderate sensitivity to parameter selection, with performance variations of less than 10% when parameters remain within 50% of their optimal values. The optimal α/β ratio remained consistent across different noise levels, suggesting that once calibrated, the same parameter configuration can be used across varying clinical conditions.

5.3 Multi-modal CVD Detection with ECG, PCG and the NMCSE-Estimated Coupling Signal Using TSFE Network

We evaluated the effectiveness of integrating the NMCSE-estimated coupling signal for CVD detection through two sets of experiments: an ablation study examining the contribution of each modality and a comparison with state-of-the-art multi-modal approaches.

Ablation Experiment We first conducted an ablation study to assess the contribution of each modality to classification performance. The experiment involved individually using ECG, PCG, and the NMCSE-estimated coupling signal as inputs to the TSFE network. We also evaluated a dual-modal setup (ECG+PCG) and the complete multi-modal configuration (ECG+PCG+coupling signal).

Table 4: Evaluation metrics for different input configurations.

Input Configuration	Accuracy (%)	Specificity (%)	Sensitivity (%)	AUC
Single ECG	81.23	77.25	85.27	0.86
Single PCG	84.71	81.92	89.87	0.89
NMCSE-estimated coupling	90.25	87.48	94.13	0.93
ECG + PCG	93.85	93.02	94.67	0.96
All three modalities	97.38	97.15	97.92	0.98

As shown in Table 4, among single-modal inputs, the NMCSE-estimated coupling signal achieved the highest performance (90.25% accuracy, 0.93 AUC), outperforming both ECG (81.23%) and PCG (84.71%) alone. This demonstrates that the coupling signal effectively captures the cross-modal relationship between electrical and mechanical cardiac activities.

The dual-modal configuration (ECG+PCG) improved accuracy to 93.85%, confirming the complementary nature of these modalities. However, the complete multi-modal approach further increased performance to 97.38% accuracy and 0.98 AUC, highlighting the added value of the coupling signal in capturing electromechanical dynamics not fully represented by ECG and PCG individually.

Table 5: Performance comparison with existing methods.

Method	Accuracy (%)	Specificity (%)	Sensitivity (%)	AUC
Li et al. [18]	86.67	82.48	88.37	0.91
Hettiarachchi et al. [12]	81.94	77.21	84.87	0.88
Li et al. [17]	74.28	62.69	87.17	0.81
Li et al. [16]	88.33	92.15	84.92	0.93
Sun et al. [22]	95.38	87.38	100.00	0.97
Zhang et al. [24]	94.38	92.38	84.38	0.97
NMCSE + TSFE (ours)	97.38	97.15	97.92	0.98

Comparison with Existing Multi-Modal Methods We compared our approach with state-of-the-art multi-modal methods for CVD detection, summarized in Table 5.

Our approach outperforms existing methods across most metrics, achieving the highest overall accuracy (97.38%), specificity (97.15%), and AUC (0.98). Notably, our method surpasses Sun et al. [22], which also utilizes coupling signals but relies on deconvolution-based estimation. This performance difference (97.38% vs. 95.38% accuracy) directly demonstrates the advantage of using NMCSE for robust coupling signal estimation in noisy environments.

6 Conclusion

This paper introduced Noise-Robust Multi-Modal Coupling Signal Estimation, which reformulates ECG-PCG coupling signal estimation through optimal transport theory. By shifting from ill-posed deconvolution to well-posed distribution matching, NMCSE offers a theoretically sound framework that jointly optimizes amplitude and temporal alignment while mitigating noise amplification.

Experiments on PhysioNet Dataset with realistic hospital noise demonstrated NMCSE’s superior robustness, reducing estimation errors by approximately 30% compared to conventional methods including Tikhonov regularization, Wiener filtering, and sparsity-based approaches. When integrated with our Temporal-Spatial Feature Extraction network for multi-modal CVD detection, our approach achieved 97.38% accuracy and 0.98 AUC, outperforming state-of-the-art methods.

The noise robustness of NMCSE addresses a critical gap between theoretical possibility and clinical reality in coupling signal-enhanced diagnostic frameworks. By enabling reliable performance under realistic noise conditions, our method paves the way for wider adoption of multi-modal cardiac analysis in clinical settings. Future work will focus on real-time implementation and validation across diverse patient populations with varying cardiac conditions to further establish its clinical utility.

References

1. Akay, Y.M., Akay, M., Welkowitz, W., Semmlow, J.L., Kostis, J.B.: Noninvasive acoustical detection of coronary artery disease: a comparative study of signal processing methods. *IEEE Transactions on Biomedical Engineering* **40**(6), 571–578 (1993)
2. Al-Makki, A., DiPette, D., Whelton, P.K., Murad, M.H., Mustafa, R.A., Acharya, S., Beheiry, H.M., Champagne, B., Connell, K., Cooney, M.T., et al.: Hypertension pharmacological treatment in adults: a world health organization guideline executive summary. *Hypertension* **79**(1), 293–301 (2022)
3. Ali, S.N., Shuvo, S.B., Hasan, T.: A robust deep learning framework for real-time denoising of heart sound. *TechRxiv* (2022)
4. Alkhodari, M., Fraiwan, L.: Convolutional and recurrent neural networks for the detection of valvular heart diseases in phonocardiogram recordings. *Computer Methods and Programs in Biomedicine* **200**, 105940 (2021)
5. Berkaya, S.K., Uysal, A.K., Gunal, E.S., Ergin, S., Gunal, S., Gulmezoglu, M.B.: A survey on ecg analysis. *Biomedical Signal Processing and Control* **43**, 216–235 (2018)
6. Clifford, G.D., Liu, C., Moody, B., Springer, D., Silva, I., Li, Q., Mark, R.G.: Classification of normal/abnormal heart sound recordings: The physionet/computing in cardiology challenge 2016. In: 2016 Computing in cardiology conference (CinC). pp. 609–612. *IEEE* (2016)
7. Dong, H., Wang, X., Li, Y., Sun, C., Jiao, Y., Zhao, L., Zhao, S., Xing, M., Zhang, H., Liu, C.: Non-destructive detection of cad stenosis severity using ecg-pcg coupling analysis. *Biomedical Signal Processing and Control* **86**, 105328 (2023)
8. Gaikwad, K.M., Chavan, M.S.: Removal of high frequency noise from ecg signal using digital iir butterworth filter. In: 2014 IEEE Global Conference on Wireless Computing & Networking (GCWCN). pp. 121–124. *IEEE* (2014)

9. Giddens, D., Mabon, R., Cassanova, R.: Measurements of disordered flows distal to subtotal vascular stenoses in the thoracic aortas of dogs. *Circulation Research* **39**(1), 112–119 (1976)
10. Habetha, J.: The myheart project-fighting cardiovascular diseases by prevention and early diagnosis. In: 2006 international conference of the IEEE engineering in medicine and biology society. pp. 6746–6749. IEEE (2006)
11. Han, H., Xiang, M., Lian, C., Liu, D., Zeng, Z.: A multimodal deep neural network for eeg and pcg classification with multimodal fusion. In: 2023 13th International Conference on Information Science and Technology (ICIST). pp. 124–128. IEEE (2023)
12. Hettiarachchi, R., Haputhanthri, U., Herath, K., Kariyawasam, H., Munasinghe, S., Wickramasinghe, K., Samarasinghe, D., De Silva, A., Edussooriya, C.U.: A novel transfer learning-based approach for screening pre-existing heart diseases using synchronized eeg signals and heart sounds. In: 2021 IEEE international symposium on circuits and systems (ISCAS). pp. 1–5. IEEE (2021)
13. Huang, Q., Yang, H., Zeng, E., Chen, Y.: A deep-learning-based multi-modal eeg and pcg processing framework for label efficient heart sound segmentation. In: 2024 IEEE/ACM Conference on Connected Health: Applications, Systems and Engineering Technologies (CHASE). pp. 109–119. IEEE (2024)
14. Khan, F.A., Abid, A., Khan, M.S.: Automatic heart sound classification from segmented/unsegmented phonocardiogram signals using time and frequency features. *Physiological measurement* **41**(5), 055006 (2020)
15. Li, H., Ren, G., Yu, X., Wang, D., Wu, S.: Discrimination of the diastolic murmurs in coronary heart disease and in valvular disease. *IEEE Access* **8**, 160407–160413 (2020)
16. Li, H., Wang, X., Liu, C., Li, P., Jiao, Y.: Integrating multi-domain deep features of electrocardiogram and phonocardiogram for coronary artery disease detection. *Computers in Biology and Medicine* **138**, 104914 (2021)
17. Li, J., Ke, L., Du, Q., Chen, X., Ding, X.: Multi-modal cardiac function signals classification algorithm based on improved ds evidence theory. *Biomedical Signal Processing and Control* **71**, 103078 (2022)
18. Li, P., Hu, Y., Liu, Z.P.: Prediction of cardiovascular diseases by integrating multi-modal features with machine learning methods. *Biomedical Signal Processing and Control* **66**, 102474 (2021)
19. Liu, C., Springer, D., Li, Q., Moody, B., Juan, R.A., Chorro, F.J., Castells, F., Roig, J.M., Silva, I., Johnson, A.E., et al.: An open access database for the evaluation of heart sound algorithms. *Physiological measurement* **37**(12), 2181 (2016)
20. Rangayyan, R.M., Lehner, R.J.: Phonocardiogram signal analysis: a review. *Critical reviews in biomedical engineering* **15**(3), 211–236 (1987)
21. Sun, C., Liu, C., Wang, X., Liu, Y., Zhao, S.: Coronary artery disease detection based on a novel multi-modal deep-coding method using eeg and pcg signals. *Sensors* **24**(21), 6939 (2024)
22. Sun, C., Liu, X., Liu, C., Wang, X., Liu, Y., Zhao, S., Zhang, M.: Enhanced cad detection using novel multi-modal learning: Integration of eeg, pcg, and coupling signals. *Bioengineering* **11**(11), 1093 (2024)
23. Tafur, E., Cohen, L.S., Levine, H.D.: The normal apex cardiogram: Its temporal relationship to electrical, acoustic, and mechanical cardiac events. *Circulation* **30**(3), 381–391 (1964)
24. Zhang, H., Zhang, P., Lin, F., Chao, L., Wang, Z., Ma, F., Li, Q.: Co-learning-assisted progressive dense fusion network for cardiovascular disease detection using eeg and pcg signals. *Expert Systems with Applications* **238**, 122144 (2024)